Advances in Industrial and Manufacturing Engineering 3 (2021) 100056

Contents lists available at ScienceDirect

Advances in Industrial and Manufacturing Engineering

journal homepage: www.sciencedirect.com/journal/advances-in-industrial-and-manufacturing-engineering

Glass precision micro-cutting using spark assisted chemical engraving

Lucas Abia Hof [a,*], Rolf Wuthrich [b,**]

[a] Department of Mechanical Engineering, École de Technologie Supérieure, 1100 Rue Notre-Dame O., Montréal, Québec, H3C 1K3, Canada
[b] Department of Mechanical Industrial and Aerospace Engineering, Concordia University, 1455 de Maisonneuve Blvd. West, Montreal, Quebec, H3G 1M8, Canada

ARTICLE INFO

Keywords:
Free-form micro-cutting
Glass
Mass-personalization
Spark assisted chemical engraving (SACE)
Micro-fabrication
Rapid prototyping

ABSTRACT

Manufacturing industry faces new challenges with the emergence of the need for the production of small batches of personalized parts. Such production methods demand for a capability to integrate multiple machining operations in one manufacturing process to reduce setup and calibration time and tooling costs. This requirement is especially challenging for difficult-to-machine materials such as glass, since there exist only a limited number of glass machining technologies and further these technologies often require specialized tooling. Glass cutting is among the crucial machining operations, which is frequently required for glass products.

The presented study discusses free-form micro-cutting by Spark Assisted Chemical Engraving (SACE), determining cut parameters, in terms of tool feed-rate F and depth-of-cut p in function of machining voltage. A simple model is discussed allowing to predict the maximal product $F{\cdot}p$ which can be used to cut glass by SACE. The presented data and model allow to reduce the time-consuming trial and error process in determining appropriate cutting parameters. An interesting finding is that lowest cutting times can be achieved with tools of 100-μm diameter. Cut surface roughness of initial cuts can be reduced by deploying subsequently incremental finishing (polishing) passes performed at lower machining voltage, lower tool feed rates and higher angular tool rotation. It is demonstrated that very smooth cut surfaces (Rz ~ 1 μm) can be achieved.

1. Introduction

Since recently, manufacturing industry faces new challenges with the emergence of the need for the production of small batches of personalized parts (El Maraghy and El Maraghy, 2014; Aheleroff et al., 2019). In personalized parts, where the customer is actively involved in the design process, manufacturing must be able to accommodate the geometry changes in an economically viable manner (Hu, 2013). This paradigm demands new manufacturing processes keeping minimal manufacturing overhead for a change of part geometries. In particular, the ability to incorporate multiple operations in one manufacturing process to reduce setup and calibration time and tooling costs is key for such mass-personalization production methods (Hof, 2018). The adoption to mass personalized manufacturing, is especially challenging for difficult-to-machine materials as there exist only a limited number of technologies able to machine them and these technologies often need specialized tooling. Glass is a typical example of a difficult-to-machine material. For centuries, glass has been used to fabricate glazing and containers. The used manufacturing technologies are usually based on blowing and molding involving specialized tooling (Le Bourhis, 2014). More recently, glass started to be used for new applications appearing in high-end products such as displays (e.g. smartphones, smartwatches), Micro-Electro-Mechanical-System (MEMS) and Optical-Electro-Mechanical-Systems (OEMS) devices (Hèulsenberg et al., 2008; Le Bourhis, 2014). The use of glass in these high-tech applications is essentially motivated due to the numerous qualities of glass including its optical transparency, bio- and chemical inertness, mechanical strength and hardness, thermal properties and its recyclability. In addition, glass is radio-frequency transparent, which makes it a suitable material for sensor and energy transmission devices. Glass's relatively high resistance to heat and its low coefficient of thermal expansion (e.g. Zerodur, Schott) makes it an appealing material for high temperature microfluidic MEMS devices (Whitesides, 2006) (e.g. used in oil industry research (Sinton, 2014)) and for microfluidic bio-applications as sterilization by autoclaving is possible (Whitesides, 2006).

Nevertheless, glass is still difficult to machine by available technologies. This is largely due to its brittle nature, its chemical resistance and

* Corresponding author.
** Corresponding author.
E-mail addresses: lucas.hof@etsmtl.ca (L.A. Hof), rolf.wuthrich@concordia.ca (R. Wuthrich).

https://doi.org/10.1016/j.aime.2021.100056
Received 30 March 2021; Received in revised form 14 June 2021; Accepted 3 July 2021
Available online 6 July 2021

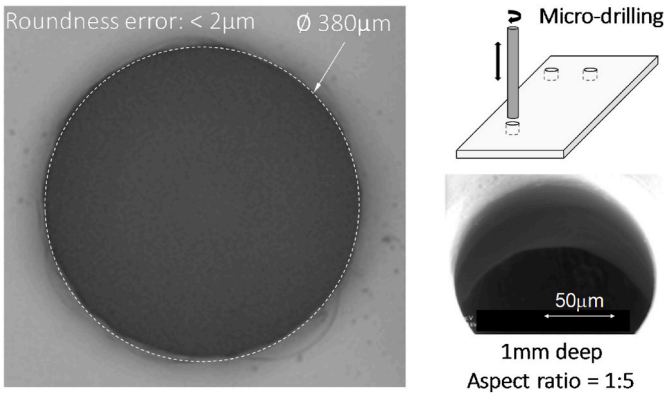

Fig. 1. SACE machined micro-holes in glass with low roundness error (<2 µm) machined by the industrial Microfor SACE machine developed together with Posalux SA (Posalux S.A..)).

its relatively high thermal conductivity. Most commonly multiple technologies need to be deployed to manufacture a glass-based product (Hèulsenberg et al., 2008; Le Bourhis, 2014; Swift Glass Company). There exist a wide range of glass machining technologies for drilling, milling, cutting, and polishing, which can be categorized in four groups; thermal, mechanical, chemical and hybrid processes with each their own advantages and limitations on machining (Hof and Abou Ziki, 2017). However, most often each technology is able to perform only one or few types of operations. Spark Assisted Chemical Engraving (SACE), also referred to as Electrochemical Discharge Machining (ECDM) (Basak and Ghosh, 1996), is among the few that can perform various types of machining operations on a same setup reducing dramatically issues related to calibration (Hof, 2018; Hof and Wüthrich, 2017). SACE is a hybrid machining process in which localized glass etching is promoted by a heat source generated electrochemically around a tool electrode. Historically first developed in Japan for micro-drilling (Tutui, 1960; Kurafuji and Suda, 1968), SACE has later been extended to other operations such as micro-channel machining (Jui et al., 2013; Cao et al., 2009) and fabrication of 2.5D microstructures (Jui et al., 2013; Zheng et al., 2007). Precision and quality has improved dramatically as development were pushed further. A significant improvement was achieved by introducing pulsed voltage machining (Cao et al., 2009; Zheng et al., 2007; Kim et al., 2006) and by using optimized tool shapes (Han et al., 2008; Wei et al., 2010; Yang et al., 2011). Micro channel machining (Van Toan et al., 2016) and micro-drilling (Hof and Abou Ziki, 2017) (Razfar et al., 2014; Maillard et al., 2007) by SACE has been extensively characterized and is routinely applied. Fig. 1 presents the excellent quality (sharp edges with almost no burrs) and high precision (low roundness error < 0.5%) that can be achieved by micro-drilling using SACE technology. However, the capability of SACE to perform micro-cutting is much less studied. The present contribution aims to investigate systematically machining parameters to achieve micro-cutting over a significant thickness.

Glass cutting is a crucial machining operation, which is frequently required for glass products (Dudutis et al., 2020; Nisar et al., 2013). A typical example is the die-singularizing operation in the fabrication of glass microchips, which is presently essentially done by diamond saw cutting (dicing) (Li et al., 2019; Zhou et al., 2006) and as such is limited to simple geometries (e.g. rectangular shapes) with relatively poor surface finish and chipping of the cut edges, resulting in the need of added post-processing steps (e.g. mechanical grinding (Xie et al., 2016) and polishing (Dudutis et al., 2019)). In fact, conventional glass cutting methods, such as mechanical dicing and score and break are still widely employed by industry as they are simple to use and cost-effective (Pan et al., 2008; Nisar et al., 2013). Laser scribe and break methods were introduced and improved (Dudutis et al., 2019) to address the surface finish of the cut section, however the limitations on geometry of cut persist. Other non-conventional glass cutting techniques, such as 1) hot-air jet cutting (Prakash et al., 2001), 2) waterjet cutting (Salinas-Luna et al., 2006) and 3) laser cutting (Nisar et al., 2013) offer more flexibility on cutting geometries, but they are limited by respectively 1) low cutting speed, limited to relatively thick glass (2–20 mm), requiring an initial scratch for crack initiation (two-stage process), 2) requiring post-process cleaning and mechanical grinding, high investment and maintenance cost, relatively low precision tolerance (±200 µm) and 3) being glass-type specific processes (i.e. not versatile) imply high initial setup costs and relatively poor reliability. An interesting advantage of using SACE technology for precision cutting of glass is its ability to perform *free-form* cutting operations with relatively high-quality finish of the surface of cut. Free-form cutting remains challenging for most glass machining technologies. This feature has the potential to open up a wide range of new possibilities for using glass in innovative dedicated precision applications.

Contrary to SACE glass micro-hole drilling, which is well researched by academia (Cao et al., 2009; Hof and Abou Ziki, 2017) with well-defined drilling strategies (Wüthrich et al., 2006a; Wüthrich, 2006b) requiring force feedback controlled tool electrodes (Wüthrich et al., 2000; Abou Ziki, 2014), no models relating SACE process input parameters to material removal rate are available for glass cutting. Such models are an essential requirement for reducing setup time and the development of digital twins (Aheleroff et al., 2020) for agile digital manufacturing approaches to fabricate highly personalized parts at mass-fabrication efficiency (Lafou et al., 2016; Stemmler et al., 2016). As of today, many time-consuming trial and error runs are needed to determine most suitable process parameters (e.g. machining voltage, depth-of-cut and feed rate) for milling and cutting.

The present work aims to investigate systematically SACE micro-cutting. Using empirical data, a quantitative model is developed which allows to determine maximal depth-of-cut and tool feed rates enabling the operator to choose adequate machining parameters without lengthy trial and error process. As such, this developed model adds to address the

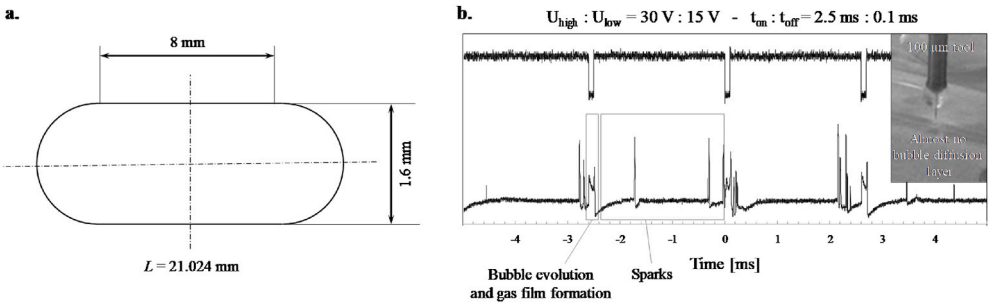

Fig. 2. a. Oval toolpath design for the glass cutting experiments. **b.** Pulsed voltage machining settings with pulse-high time $t_{on} = 2.5$ ms and pulse-low time $t_{off} = 0.1$ ms. The pulse low is set at $U_{low} = 15$ V and the pulse high value here is $U_{high} = 30$ V. Note the absence of a bubble diffusion zone upon applying the low pulse off time value.

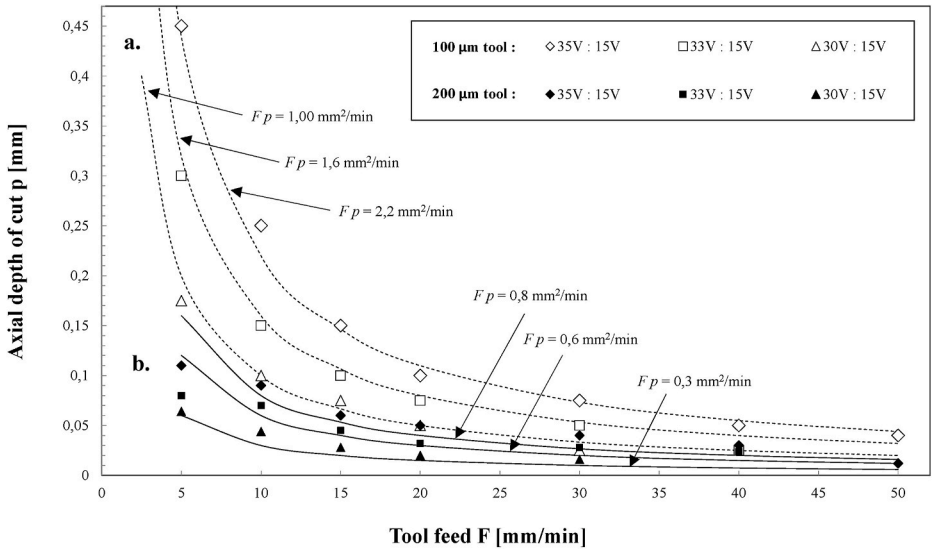

Fig. 3. Experimental values obtained for maximal depth-of-cut p (mm) against tool feed-rate F (mm/min.). **a.** Values for 100 µm diameter tungsten carbide tools are represented by the non-filled markers. The dashed lines represent the product $F \bullet p$. **b.** Values for 200 µm diameter tungsten carbide tools are represented by the filled markers.

demand for high-level integration strategies across the full manufacturing cycle, from part design to fabrication of a high-precision product, which is a critical tool for mass-personalization manufacturing processes by reducing machining overhead.

Furthermore, Spark Assisted Chemical Polishing (SACP) is introduced as a complementary finishing approach to reduce glass cut-surface roughness. Significant cut surface quality improvements have been achieved deploying SACP by re-machining a SACE machined surface of cut by small lateral increments (e.g. 2 µm) of the tool electrode at low machining voltage. The reported SACP finishing method can achieve cutting surfaces of absolute roughness values R_z below 1 µm.

2. Materials and methods

Machining operations were conducted on a commercial Posalux SACE machine (Posalux S.A. n.d.). This machining centre incorporates a force sensor able to detect axial forces down to a few milli-Newton (mN) while rotating the tool (Wuthrich et al., 2017). The used cylindrical tools were made of tungsten carbide with 100 µm and 200 µm diameters. A tool rotation rate of 1000 rpm was used. As electrolyte, 30 wt% Potassium Hydroxide (KOH) solution, prepared using deionized water, was deployed. Work-pieces were 0.4 mm thick MEMpax® (Schott) glass slides. To investigate machining parameters for cutting, an oval type shape was cut out of the glass (Fig. 2 a). Machining parameters were machining voltage, tool feed-rate F and depth-of-cut p. Pulsed voltage machining was used with pulse high time of 2.5 ms and pulse low time of 0.1 ms (Fig. 2 b). The pulse low value was kept at 15 V and for the pulse high values 35, 33 and 30 V were used. Using pulsed voltage is critical to ensure control over the sparking process. The low voltage phase is crucial to allow cooling of the tool and work-piece. On one hand, a sufficiently low voltage is needed to permit cooling and on the other hand this low voltage value should be high enough to allow flushing of the machining zone (via the bubble evolution taking place on the tool surface) and to minimize the appearance of a short anodic pulse which would lead to excessive tool wear. The on-time has further to be short enough to keep a stable gas film (less than gas film life time) to ensure a stable sparking process.

2.1. Machining strategy was as follows

- First the position of the glass surface (workpiece) was measured by the SACE machine (using the incorporated profilometer with an accuracy of 1 µm);
- A first path, a few microns (less than 5 µm) above the glass surface, was traced at tool feed-rate F with the pulsed voltage turned on;
- Subsequent paths were then executed with a depth of cut p until the workpiece was entirely cut. The cut was considered successful if the entire cut could be performed without measuring any axial force on the tool.

Note that, in the framework of the described machining strategy, the cut of depths is defined differently than the usual definition of depth of cut as used, for example, in conventional milling processes. Indeed, the tool is always above the workpiece surface and does not plunge into it.

The produced cut surfaces were qualitatively evaluated by optical microscopy (Keyence VHX 5000) and electronic microscopy (Scanning Electron Microscope (SEM), variable pressure - Hitachi S–3400N.

3. Results and discussion

3.1. SACE micro-cutting

Fig. 3. a shows, for a cylindrical 100 µm diameter tool, the maximal depth of cut p that can be deployed for successful cutting for a given tool feed-rate F and machining voltage. Lower depths of cut result in successful machining whereas higher values will lead to mechanical contact with the workpiece resulting in tool bending or even breaking. It can be observed that for a given machining voltage, the product $F \bullet p$ is constant (dashed lines on Fig. 3).

That the product $F \bullet p$ is a constant for a given machining voltage can be explained by keeping in mind the material removal mechanism in SACE. In SACE glass machining, material removal is achieved by high temperature etching (Abou Ziki et al., 2015; Wüthrich and Abou Ziki, 2015; Yang et al., 2001). The local temperature must reach a critical value T_m in order machining can take place. If flushing of the machining zone is effective, then material removal rate will only be limited by the heat propagation inside the glass workpiece (explicitly: 1) etch rates are significantly faster than the rate of propagation of heat inside the workpiece, 2) the electrolyte can always reach the machining zone

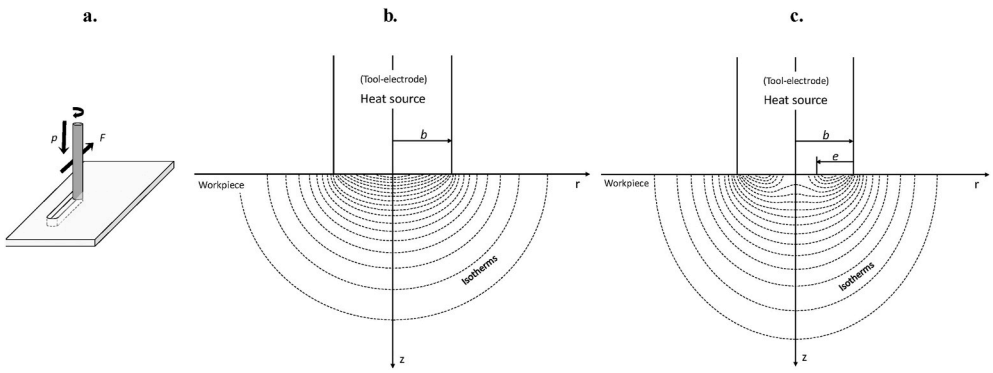

Fig. 4. a. Schematic representation of SACE micro-cutting, when cutting with a rotating tool electrode (radius r) at tool feed-rate F and an axial depth-of-cut p. **b.** Temperature distribution for SACE machining for a homogenous disk source. The required heat power, to locally heat the workpiece, is provided by a cylindrical uniform disk heat source with radius b (the dotted lines are the isotherms $T = T_m$ for specific time intervals). **c.** Temperature distribution for SACE machining for a homogenous ring heat source. The needed heat power to locally heat the workpiece is provided by a cylindrical homogenous ring (thickness e) heat source.

quickly and 3) etched material is efficiently removed from the machining zone) (Abou Ziki et al., 2015; Wüthrich and Abou Ziki, 2015).

The electrical discharges between tool and electrolyte across the gas film act as heat source that will locally increase the temperature of the workpiece. Let $\dot{h}$ be the rate of propagation inside the glass workpiece of the isotherm $T = T_m$. As the tool moves forward during machining (Fig. 4 a), it will heat locally the workpiece during the typical time $\Delta t = d/F$ Δt = d/F, where d is the diameter of the tool. In this time, the isotherm T_m will have reached a depth of about $\Delta t \cdot \dot{h} = d\dot{h}/F$ (Fig. 4 b and 4 c). If this distance is smaller than the depth of cut, not enough material will be etched away in order to allow in the next path to successfully continue the cutting operation. Note that during cutting, contrary to drilling, flushing of the machining zone is not a problem and consequently it will not limit the machining rate (to further ensure excellent flushing of the machining zone, a tool rotation of 1000 rpm was used). In summary, one has to machine at a maximal depth of cut p satisfying:

$$F \cdot p \leq d \cdot \dot{h} \tag{1}$$

Note that for a given constant product $F \bullet p$, the overall cutting time for a part will be the same. Indeed, cutting time t for a cut of length L and height h is given by:

$$t = \frac{L \cdot h}{F \cdot p} \tag{2}$$

As for a given workpiece, tool and machining voltage the product $d \cdot \dot{h}$ is fixed, the maximal depth of cut p_{max} for a certain tool feed-rate F must satisfy:

$$F \cdot p_{max} = d \cdot \dot{h} = \text{ constant} \tag{3}$$

For practical implementation of SACE cutting, equation (3) is very valuable. One can determine the constant $d \cdot \dot{h}$ for different machining voltages. In the reminder of the paper, we will refer to this constant as the SACE micro-cutting constant. Once these constants are tabulated, one can directly select the machining parameters F and p accordingly. Note that according to Equation (2) a given choice of the micro-cutting constant $F \bullet p$ determines the overall cutting time. In principle any combination of F and p (as long as (3) is satisfied) would give a same machining time. However, quality will differ as will be discussed later.

To estimate the micro-cutting constant, the calculation of $\dot{h}$ is required. A simple model is presented to achieve this. Fig. 4 gives an overview of micro-cutting in SACE. The tool is considered as a heat source which will heat locally the workpiece. For tools with sufficiently small diameter, one can approximate this heat source as a disk source (Fig. 4 b). Such model was first proposed by Gosh et al. (Basak and Ghosh, 1996) and further developed to explain the observed drilling rates in function of the SACE machining parameters (Jalali et al., 2009; Wüthrich and Abou Ziki, 2015). In this model, the rate of propagation of the isotherm $T = T_m$ is given by:

$$\dot{h} = \frac{4a}{d} \frac{\kappa - 1}{\kappa} \left[1 - \exp\left(- \frac{\pi(\kappa - 1)^2}{\kappa^2} \right) \right] \tag{4}$$

with κ the normalized heat power defined as the ratio between the generated heat power during machining and minimal heat power needed in order machining can occur. The parameter a is the thermal diffusivity of the workpiece material (here: $a \approx 6 \bullet 10^{-7}$ m^2/s typically for glass (Yang et al., 1992)).

Consequently, for tools small enough such that the approximation of a homogenous disk heat source (Fig. 4 b) is acceptable, the cutting parameters must satisfy:

$$F \cdot p \leq 4a \frac{\kappa - 1}{\kappa} \left[1 - \exp\left(- \frac{\pi(\kappa - 1)^2}{\kappa^2} \right) \right] \tag{5}$$

Note that under these conditions, the maximal value $[F \cdot p]_{max}$ of the micro-cutting constant is not a function of the tool diameter, and consequently the minimal cutting time, does not depend on neither on the tool diameter.

Using estimations for κ in function of the machining voltages reported in the literature (Jalali et al., 2009), one finds that for 30 V (κ = 1.15) $[F \cdot p]_{max}$ = 1.0 mm^2/min, for 33 V (κ = 1.18) one finds $[F \cdot p]_{max}$ = 1.6 mm^2/min and for 35 V (κ = 1.20) one obtains $[F \cdot p]_{max}$ = 2.2 mm^2/min. These values are used in Fig. 3 to draw the dashed lines for the 100 µm tool. An excellent agreement of the empirical tool feed and depth-of-cut values with these lines can be observed.

However, as observed on Fig. 3, for larger tool diameters (200 µm; Fig. 3 b), the values of $[F \cdot p]_{max}$ do no longer agree with equation (5) and machining becomes significantly slower. The reason is that the hypothesis of the homogenous disk heat source is no longer acceptable. In fact, as the sparks (which are the heat source) are mainly emitted from the edges of the tool bottom (circular perimeter), the hypothesis of a uniform heat source is questionable for large tools.

A better approximation for the heat source, in the case of larger tools, is a ring heat source (thickness e of the ring with outer diameter b as shown in Fig. 4c). To explore if the main reason behind the reduced SACE glass cutting speed is the change in geometry of the heat source, a numerical model was used. Therefore, Matlab® PDE toolbox (Mathworks, 2016) was used to solve the normalized transient two-dimensional heat problem (normalized temperature $\overline{T} = \frac{T - T_o}{P_o/(\lambda \pi b)}$, where P_o is the heat source power, T_o is the temperature at infinity, λ is the thermal conductivity of the workpiece, and the normalized time $\bar{t} = \frac{4a}{b^2} t$; see (Hof, 2018) for details of the numerical simulation):

$$4 \cdot \frac{\partial \overline{T}}{\partial \bar{t}} = \nabla^2 \overline{T} \tag{6}$$

with a ring heat source and normalized boundary conditions:

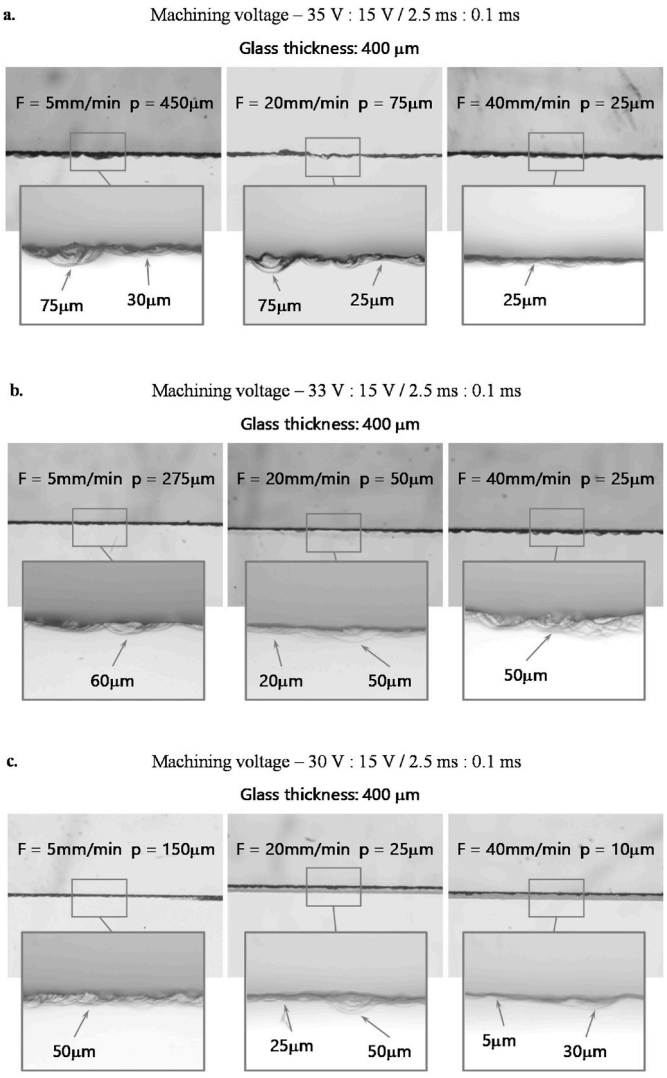

Fig. 5. Optical microscope images of SACE cut quality on glass samples (Mempax®, Schott). SACE cutting was performed using 100 µm diameter tungsten carbide tools, at different machining voltage, feed-rate F and depth-of-cut p. **a.** SACE glass cuts at high pulsed voltage (35 V). **b.** SACE glass cuts using medium pulsed voltage (33 V). **c.** SACE glass cuts deploying low pulsed voltage (30 V).

$$\frac{\partial \overline{T}}{\partial \overline{z}}\left(\overline{r},\overline{z}=0,\overline{t}\right)=\begin{cases}0, & \overline{r}>1\\ -\left[\dfrac{1}{1-\left(1-\dfrac{e}{b}\right)^2}\right], & \overline{r}\le 1\end{cases} \tag{7}$$

where $\overline{z}=\frac{z}{b}$ is the normalized z-coordinate and $\overline{r}=\frac{r}{b}$.

The numerical solution of this heat problem allows to determine $\dot{h}$, the rate of propagation inside the glass workpiece of the isotherm $T=T_m$, for a homogenous ring heat source. The numerical solutions show that if $e/b=0.9$ to 0.95 (i.e. the centre of the larger tool is not efficient in providing a heat source), the results from Fig. 3b can be well matched with equation (1).

Using this numerical model for $e/b=0.92$ the maximal SACE micro-cutting constants $[F{\cdot}p]_{max}$ for the various voltages are now: for 30 V ($\kappa=1.15$) $[F{\cdot}p]_{max}=0.3$ mm^2/min, for 33 V ($\kappa=1.18$) $[F{\cdot}p]_{max}=0.6$ mm^2/min and for 35 V ($\kappa=1.20$) $[F{\cdot}p]_{max}=0.8$ mm^2/min. These values are in reasonable good agreement with the experimental observations (Fig. 3 b).

Hence, the reduction of SACE glass micro-cutting speed is mostly due to the changed geometry of the heat source. The heat source efficiency is rapidly decreased when deploying larger diameter tools (since then the tool no longer acts as a homogenous disk heat source, i.e. $\frac{e}{b}<1$) which affects negatively the machining speed. As shown in Fig. 3b, the machining feed rate is already reduced by a factor of ~ 3–4 upon using a 200 µm diameter tool. On the other hand, deploying tools smaller than 100 µm diameter will not contribute to increased machining efficiency as in this case the heat source can already be considered as a homogenous disk heat source, and as shown by Equation (5) cutting time becomes independent of the tool diameter. In summary one can conclude that using 100 µm is optimal in terms of machining time for a given cutting path.

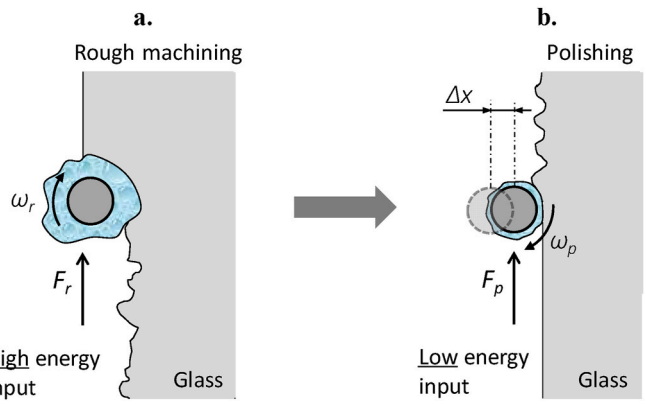

Fig. 6. Cutting followed by re-machining in order to reduce the roughness of micro-cuts. **a.** Initial rough cut (machining voltage U_{high}/U_{low}, tool feed-rate F_r and tool rotation ω_r.) **b.** Succeeding polishing step with a displacement Δx towards the glass surface with machining parameters $U_{p,high}/U_{p,low}$, F_p and ω_p.

The cuts were further characterized qualitatively using optical microscopy. Fig. 5 compares different cuts with various cutting parameters. Lower machining voltage leads to enhanced cut quality. Generally, using higher tool feed rates with lower cutting depths results as well in slightly improved machining quality. Overall, in terms of quality, it is preferable to cut at low cutting depths and high tool feed rate rather than high cutting depths and low tool feed rate. However, the improvement remains minor. As practical window of best cutting parameters to use, it is suggested to choose intermediate feed rates with their corresponding cutting depths, i.e. tool feed rates ranging from 15 to 25 mm/min are recommended. For applications requiring higher quality (less variation in surface smoothness), a methodology for a finishing pass is required.

3.2. Spark Assisted Chemical Polishing (SACP)

Criteria (3) discussed in section 3.1, allows to select appropriate cutting parameters for glass micromachining with SACE. In general, using a small depth-of-cut combined with low voltages results in better quality cuts. Still, there is room for improvement and several applications will require better cuts. In order to achieve better cut quality, a two-step strategy - Spark Assisted Chemical Polishing (SACP) – is proposed. First, a rough cut is executed. Secondly, using lower machining voltage (lower than the one that would allow to achieve a cut) are used to re-machine the cut and smoothen its surface. As the voltage is lower, the tool will be moved by a lateral distance Δx relative to the cutting trajectory, towards the glass surface (Fig. 6). This second step will be referred to as the "polishing step" in this paper. Several of such polishing paths may be required to achieve the desired cut quality.

During the second step, besides using a lower machining voltage, which results in less aggressive machining, a higher tool rotation than in cutting is used in order to create a forced, more uniform, electrolyte flow. The rationale is to achieve conditions similar to chemical etching. In such conditions material removal rates is low, which is desired in order to remove only a relatively small amount of glass from the roughly

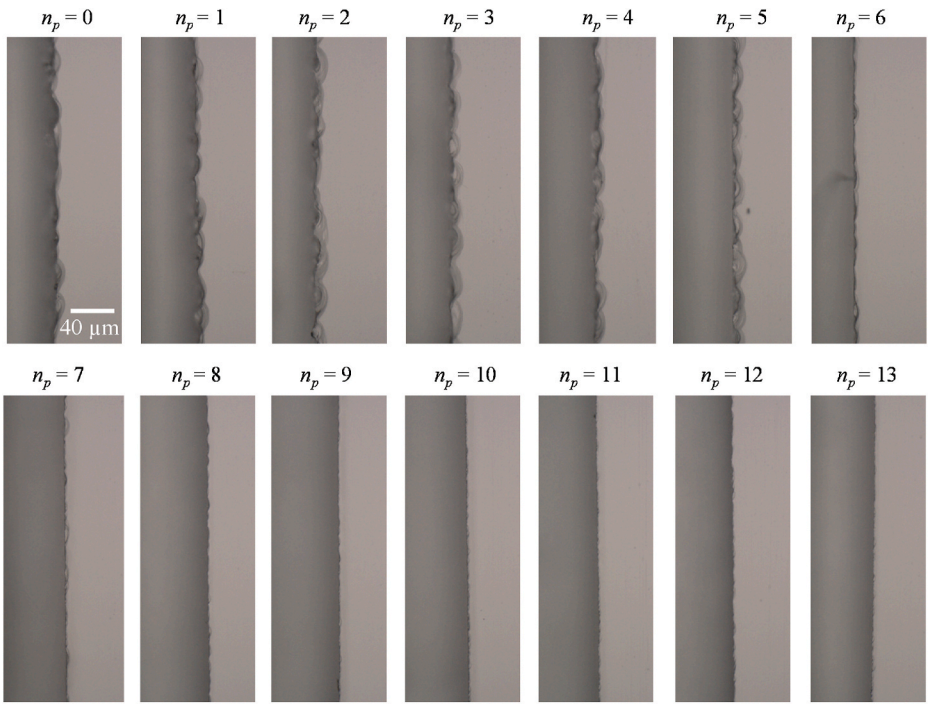

Fig. 7. Micro-cut in glass by SACE followed by n_p polishing passes ($n_p = 0$ is the initial rough cut; machining parameters: U_{high}: U_{low} = 38 V: 15 V, T_{on}: T_{off} = 2.5 ms: 0.1 ms, F_r = 15 mm/min and ω_r = 500 rpm). The polishing passes were performed at $U_{p,high}$: $U_{p,low}$ = 23 V: 15 V, T_{on}: T_{off} = 2.5 ms: 0.1 ms, F_p = 5 mm/min and ω_p = 1000 rpm.

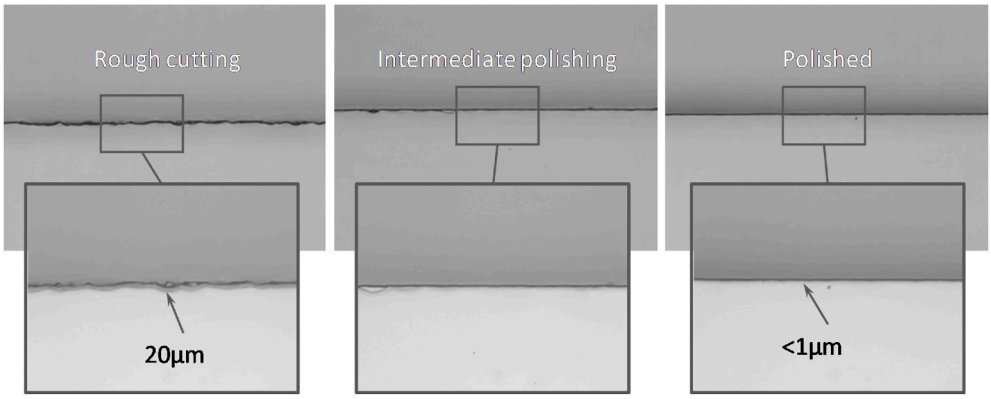

Fig. 8. Optical microscopy images illustrating the evolution from rough cut surfaces ($R_z \sim 20$ µm) via medium finished glass cut surfaces to extensive polishing of glass cut surfaces ($R_z < 1$ µm).

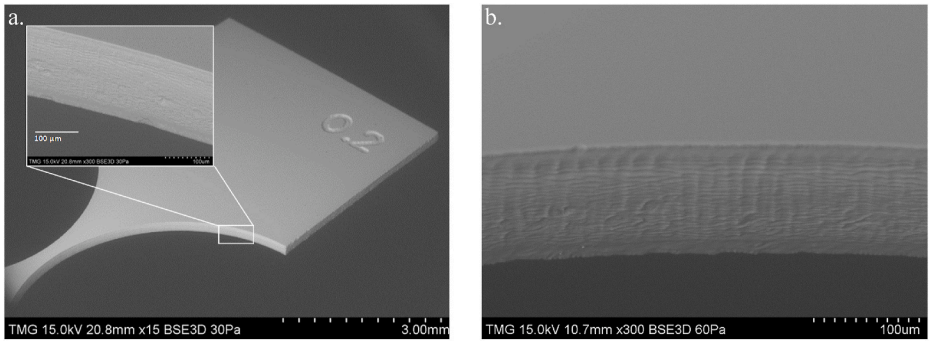

Fig. 9. SEM micrograph of a SACE cut micro-hinge out of a 200 µm thick glass (Mempax®) plate. a. Overview of the roughly cut micro-hinge, including a high magnification insert of the finished surface (curved part of the hinge). **b.** Detail of the curved cut finished by SACP after the initial rough cut.

cut surface. As the etch rate is lower than during cutting, the tool feed rate has to be reduced compared to the one used in cutting.

To define appropriate parameters for the polishing step, tests were carried where the following process parameters were investigated to assess the changes between an initial rough cut and subsequent polishing passes: polishing voltage U_p, polishing tool feed-rate F_p, tool rotation ω_p, and the displacement Δx of the tool between two finishing passes.

To demonstrate the effectiveness of the proposed SACE polishing methodology, it was chosen to start with an initial cut resulting in a high roughness ($R_z \sim 20$ µm) of the surface to be finished ($F_r = 15$ mm/min, U_{high}: $U_{low} = 38$ V:15 V; t_{on}:$t_{off} = 2.5$ ms: 0.1 ms, $\omega_r = 500$ rpm).

At first, the effect of polishing voltage was investigated. Polishing voltage amplitudes (high level $U_{p,high}$ ranging from 22 V to 29 V with increments of 1 V) were investigated for a single polishing pass with an increment Δx of 2 µm, tool feed rate F_p of 5 mm/min and tool rotation $\omega_p = 1000$ rpm. Best results were obtained by using $U_{p,high} = 23$ V.

Deploying this polishing voltage, a series of cuts were machined with increasing number n_p of polishing passes (Fig. 7). Cuts were best polished when 10 polishing passes (at fixed $\Delta x = 2$ µm) were used. Using a larger number of passes resulted in minor over-etching of the cut surface and it did not contribute to reduce further the surface roughness of the cut.

Fig. 8 shows optical microscopy images of the polished cuts. The evolution from an initial rough cut ($R_z \sim 20$ µm), passing by intermediate polished cuts, to an extensively polished cut ($R_z < 1$ µm) can be clearly observed. In this case, the cut surface absolute roughness (R_z) could be reduced by a factor of over twenty.

As an application, Fig. 9 presents a SEM micrograph of a cut micro-hinge in 200 µm thick glass. The narrow par of the hinge is 50 µm. The insert displays a detail of the polished cut (circular part of the micro-hinge). The rectangular shape holding the hinge was not polished and shows for comparison the initial rough cut surface quality. Note on how, in the insert, tiny (<5 µm) streamlines produced by the electrolyte flow around the glass cut during polishing are visible. The capability to perform free form cuts, followed by a finish step on a same machine, can contribute to open new applications for SACE cutting. As a further benefit, to be explored and quantified, it can be expected that the mechanical strength of the machined part is increased as fewer surface flaws are present in the cut, compared to a simple rough cutting.

4. Conclusion

Micro-cutting by SACE was discussed and cut parameters, in terms of tool feed-rate F and depth-of-cut p in function of machining voltage were determined. A simple model was discussed which allows to predict the maximal micro-cutting constant $F{\cdot}p$ which can be used to cut glass by SACE. The presented data and model allow to reduce the time-consuming trial and error process in determining appropriate cutting parameters. Obtained initial cuts are relatively rough ($R_z \sim 20$–50 µm).

As practical window of best cutting parameters to use, it is suggested to choose intermediate feed rates with their corresponding cutting depths, i.e. tool feed rates ranging from 15 to 25 mm/min are recommended.

An interesting finding is that lowest cutting times can be achieved with tools of 100 µm diameter. Using smaller diameter tools would not reduce further cut times, whereas using larger diameters increases significantly the time needed to cut a given shape out of glass.

The rough cuts performed by SACE can be further smoothened by using subsequently polishing passes performed at lower machining voltage and lower tool feed rates. It was demonstrated that very smooth cut surfaces ($R_z \sim 1$ µm) can be achieved. Such surfaces are required for several applications such as machining watch parts (e.g. watch glasses), speaker slots on smartphone cover glasses or artworks. Further, it was demonstrated that very fine details can be machined, by machining a micro-hinge.

The discussed model and finishing approach, introduced as Spark Assisted Chemical Polishing (SACP), contribute to the development of novel free-form and agile glass cutting processes, allowing to create new glass applications for precision applications.

Declaration of competing interest

The authors declare that they have no known competing financial interests or personal relationships that could have appeared to influence the work reported in this paper.

Acknowledgements

This work was supported by the Natural Sciences and Engineering Research Council of Canada (NSERC). The authors would also like to acknowledge Posalux SA for use of their industrial SACE machine.

References

Abou Ziki, J.D., 2014. Spark Assisted Chemical Engraving: A Novel Approach for Quantifying the Machining Zone Parameters Using Drilling Forces. Concordia University Montreal, Quebec, Canada.

Abou Ziki, J.D., Hof, L.A., Wüthrich, R., 2015. The machining temperature during spark assisted chemical engraving of glass. Manufacturing Letters 3, 9–13. https://doi.org/10.1016/j.mfglet.2014.11.003.

Aheleroff, S., Philip, R., Zhong, R.Y., Xu, X., 2019. The degree of mass personalisation under industry 4.0. Procedia CIRP 81. https://doi.org/10.1016/j.procir.2019.04.050, 1394–99.

Aheleroff, S., Zhong, R.Y., Xu, X., 2020. A digital twin reference for mass personalization in industry 4.0. Procedia CIRP 93, 228–233. https://doi.org/10.1016/j.procir.2020.04.023.

Basak, I., Ghosh, A., 1996. Mechanism of spark generation during electrochemical discharge machining: a theoretical model and experimental verification. J. Mater. Process. Technol. 62 (1–3), 46–53. https://doi.org/10.1016/0924-0136(95)02202-3.

Cao, X.D., Kim, B.H., Chu, C.N., 2009. Micro-structuring of glass with features less than 100 Mm by electrochemical discharge machining. Precis. Eng. 33 (4), 459–465. https://doi.org/10.1016/j.precisioneng.2009.01.001.

Dudutis, J., Stonys, R., Račiukaitis, G., Gečys, P., 2019. Glass dicing with elliptical bessel beam. Opt Laser. Technol. 111, 331–337. https://doi.org/10.1016/j.optlastec.2018.10.007. October 2018.

Dudutis, J., Pipiras, J., Stonys, R., Daknys, E., Kilikevičius, A., Kasparaitis, A., Račiukaitis, G., Gečys, P., 2020. In-depth comparison of conventional glass cutting technologies with laser-based methods by volumetric scribing using bessel beam and rear-side machining. Opt Express 28 (21), 32133. https://doi.org/10.1364/oe.402567.

El Maraghy, W., El Maraghy, H., 2014. A new engineering design paradigm - the quadruple bottom line. Procedia CIRP 21, 18–26. https://doi.org/10.1016/j.procir.2014.06.145.

Swift Glass Company. Industry-compliant glass drilling. https://www.swiftglass.com/glass-drilling. (Accessed 18 October 2020).

Han, M.-S., Min, B.-K., Lee, S.-J., 2008. Modeling gas film formation in electrochemical discharge machining processes using a side-insulated electrode. J. Micromech. Microeng. 18 (4), 045019 https://doi.org/10.1088/0960-1317/18/4/045019.

Hèulsenberg, D., Harnisch, A., Bismarck, A., 2008. Microstructuring of Glasses. Microstructuring of Glasses. Springer Berlin Heidelberg, Berlin, Heidelberg. https://doi.org/10.1007/978-3-540-49888-9.

Hof, L.A., 2018. High-Precision Micro-machining of Glass for Mass-Personalization. Concordia University. https://spectrum.library.concordia.ca/984180/.

Hof, L.A., Abou Ziki, J., 2017. Micro-hole drilling on glass substrates-A review. Micromachines 8 (2), 1–23. https://doi.org/10.3390/mi8020053.

Hof, L.A., Wüthrich, R., 2017. Industry 4.0 - towards fabrication of mass-personalized parts on glass by spark assisted chemical engraving (SACE). Manufacturing Letters. https://doi.org/10.1016/j.mfglet.2017.12.003.

Hu, S.J., 2013. Evolving paradigms of manufacturing: from mass production to mass customization and personalization. Procedia CIRP 7, 3–8. https://doi.org/10.1016/j.procir.2013.05.002.

Jalali, M., Maillard, P., Wüthrich, R., 2009. Toward a better understanding of glass gravity-feed micro-hole drilling with electrochemical discharges. J. Micromech. Microeng. 19 (4) https://doi.org/10.1088/0960-1317/19/4/045001.

Jui, S.K., Kamaraj, A.B., Sundaram, M.M., 2013. High aspect ratio micromachining of glass by electrochemical discharge machining (ECDM). J. Manuf. Process. 15 (4), 460–466. https://doi.org/10.1016/j.jmapro.2013.05.006.

Kim, D.J., Ahn, Y., Lee, S.H., Kim, Y.K., 2006. Voltage pulse frequency and duty ratio effects in an electrochemical discharge microdrilling process of pyrex glass. Int. J. Mach. Tool Manufact. 46 (10), 1064–1067. https://doi.org/10.1016/j.ijmachtools.2005.08.011.

Kurafuji, H., Suda, K., 1968. Electrical discharge drilling of glass. Annals of the CIRP 16, 415–419.

Lafou, M., Mathieu, L., Pois, S., Alochet, M., 2016. Manufacturing system flexibility: product flexibility assessment. Procedia CIRP 41, 99–104. https://doi.org/10.1016/j.procir.2015.12.046.

Le Bourhis, E., 2014. Glass, Mechanics and Technology. Wiley-VCH.

Li, K., Wang, Y., Zhao, Y., Jin, C., Tang, H., Zou, Q., Zhao, Y., Wang, M., 2019. High strain rate of quartz glass and its effects during high-speed dicing. Ceram. Int. 45 (10), 13523–13529. https://doi.org/10.1016/j.ceramint.2019.04.057.

Maillard, P., Despont, B., Bleuler, H., Wüthrich, R., 2007. Geometrical characterization of micro-holes drilled in glass by gravity-feed with spark assisted chemical engraving (SACE). J. Micromech. Microeng. 17 (7), 1343. http://stacks.iop.org/0960-1317/17/i=7/a=017.

Mathworks, 2016. Partial Differential Equation Toolbox User's Guide R2016a.

Nisar, S., Li, L., Sheikh, M.A., 2013. Laser glass cutting techniques—a review. J. Laser Appl. 25 (4), 042010 https://doi.org/10.2351/1.4807895.

Pan, C.T., Hsieh, C.C., Su, C.Y., Liu, Z.S., 2008. Study of cutting quality for TFT-LCD glass substrate. Int. J. Adv. Manuf. Technol. 39 (11–12), 1071–1079. https://doi.org/10.1007/s00170-007-1293-4.

Posalux, S.A.. Microfor SACE. https://www.posalux.ch/site/en/products/microfor_sace/sace. (Accessed 11 November 2020).

Prakash, E.S., Sadashivappa, K., Joseph, V., Singaperumal, M., 2001. Nonconventional cutting of plate glass using hot air jet: experimental studies. Mechatronics 11 (6), 595–615. https://doi.org/10.1016/S0957-4158(00)00033-7.

Razfar, M.R., Behroozfar, A., Ni, J., 2014. Study of the effects of tool longitudinal oscillation on the machining speed of electrochemical discharge drilling of glass. Precis. Eng. 38 (4), 885–892. https://doi.org/10.1016/j.precisioneng.2014.05.004.

Salinas-Luna, J., Machorro, R., Camacho, J., Luna, E., Nunez, J., 2006. Water jet: a promising method for cutting optical glass. Appl. Opt. 45 (15), 3477–3481. https://doi.org/10.1364/AO.45.003477.

Sinton, D., 2014. Energy: the microfluidic frontier. Lab Chip 14 (17). https://doi.org/10.1039/c4lc00267a.

Stemmler, S., Abel, D., Adams, O., Klocke, F., 2016. Model predictive feed rate control for a milling machine. IFAC-PapersOnLine 49 (12), 11–16. https://doi.org/10.1016/j.ifacol.2016.07.542.

Toan, N.V., Toda, M., Ono, T., 2016. An investigation of processes for glass micromachining. Micromachines 7 (3), 19–22. https://doi.org/10.3390/mi7030051.

Tutui, T., 1960. Electrical-discharge machining of glass. J. Jpn. Soc. Precis. Eng. 26 (309), 596–600. https://doi.org/10.2493/jjspe1933.26.596.

Wei, C., Ni, J., Hu, D., 2010. Electrochemical discharge machining using micro-drilling tools. Trans. North Am. Manuf. Res. Inst. SME 38, 105–111.

Whitesides, G.M., 2006. The origins and the future of microfluidics. Nature 442 (7101), 368–373.

Wüthrich, R., Abou Ziki, J.D., 2015. Micromachining using electrochemical discharge phenomenon. In: Micromachining Using Electrochemical Discharge Phenomenon. Elsevier. https://doi.org/10.1016/B978-0-323-24142-7.05001-0.

Wüthrich, R., Fascio, V., Viquerat, D., Langen, H., 2000. Study of spark assisted electrochemical etching - force measurements. In: International Workshop on Microfactories (IWMF 2000), 201–4. Fribourg.

Wüthrich, R., Despont, B., Maillard, P., Bleuler, H., 2006. Improving the material removal rate in spark-assisted chemical engraving (SACE) gravity-feed micro-hole drilling by tool vibration. J. Micromech. Microeng. 16 (11), N28. http://stacks.iop.org/0960-1317/16/i=11/a=N03.

Wüthrich, R., Spaelter, U., Wu, Y., Bleuler, H., 2006. A systematic characterization method for gravity-feed micro-hole drilling in glass with spark assisted chemical engraving (SACE). J. Micromech. Microeng. 16 (9), 1891. http://stacks.iop.org/0960-1317/16/i=9/a=019.

Wuthrich, R., Hof, L.A., Abou Ziki, J.D., Cusanelli, G., Thibaut, P., 2017. Spark Assisted Chemical Engraving Machine, A Workpiece Machined by the Machine, and a Process Related Thereof. WO 2017/064583 A1, issued 2017.

Xie, J., Deng, Z.J., Liao, J.Y., Li, N., Zhou, H., Ban, W.X., 2016. Study on a 5-Axis precision and mirror grinding of glass freeform surface without on-machine wheel-profile truing. Int. J. Mach. Tool Manufact. 109, 65–73. https://doi.org/10.1016/j.ijmachtools.2016.07.011.

Yang, G., Migone, A.D., Johnson, K.W., 1992. Heat capacity and thermal diffusivity of a glass sample. Phys. Rev. B 45 (1), 157–160. https://doi.org/10.1017/CBO9781107415324.004.

Yang, C.T., Ho, S.S., Yan, B.H., 2001. Micro hole machining of borosilicate glass through electrochemical discharge machining (ECDM). In: Key Engineering Materials Precision Machining of Advanced Materials, 196:149–66. Trans Tech Publications. https://doi.org/10.4028/www.scientific.net/KEM.196.149.

Yang, C.K., Wu, K.L., Hung, J.C., Lee, S.M., Lin, J.C., Yan, B.H., 2011. Enhancement of ECDM efficiency and accuracy by spherical tool electrode. Int. J. Mach. Tool Manufact. 51 (6), 528–535. https://doi.org/10.1016/j.ijmachtools.2011.03.001.

Zheng, Z.-P., Cheng, W.-H., Huang, F.-Y., Yan, B.-H., 2007a. 3D microstructuring of pyrex glass using the electrochemical discharge machining process. J. Micromech. Microeng. 17 (5), 960–966. https://doi.org/10.1088/0960-1317/17/5/016.

Zheng, Z.-P., Su, H.-C., Huang, F.-Y., Yan, B.-H., 2007b. The tool geometrical shape and pulse-off time of pulse voltage effects in a pyrex glass electrochemical discharge microdrilling process. J. Micromech. Microeng. 17 (2), 265. http://stacks.iop.org/0960-1317/17/i=2/a=012.

Zhou, M., Ngoi, B.K.A., Yusoff, M.N., Wang, X.J., 2006. Tool wear and surface finish in diamond cutting of optical glass. J. Mater. Process. Technol. 174 (1–3), 29–33. https://doi.org/10.1016/j.jmatprotec.2005.02.248.